Accelerating fronts in an electrochemical system due to global coupling

G. Flätgen and K. Krischer
Fritz-Haber-Institut der Max-Planck-Gesellschaft, Faradayweg 4-6, 14195 Berlin-Dahlem, Germany
(Received 11 July 1994; revised manuscript received 9 January 1995)

We examine spatiotemporal patterns during the reduction of peroxodisulfate to sulfate at silver ring electrodes in an electrochemical cell. The reaction displays bistable behavior in the current-voltage characteristics under potentiostatic conditions. The two stable states are characterized by different voltage drops across the double layer. We investigate transitions in the bistable region between the different states. Spatiotemporally resolved measurements of the voltage drop across the electrode-electrolyte interface show that the transition occurs via fronts. We are able to trigger these fronts by local perturbations of the electric field and thus to examine their dependence on operating parameters. It is shown that the movement of the fronts results from migration currents (movement of ions due to the electric field), and hence the system is described by reaction-migration-diffusion equations. The velocity of the fronts increases with time; hence they are accelerated. This contrasts with usual front solutions of reaction-diffusion systems, which possess a constant velocity in one-dimensional geometries. This acceleration is shown to be a consequence of a global, or more precisely nonlocal, coupling mediated through the electric field.

PACS number(s): 64.10.+h, 82.20.Mj, 82.45.+z, 47.54.+r

INTRODUCTION

Chemical waves constitute an important mechanism of transmitting information in living systems [1]. The properties of these waves are often determined by the interplay of reaction and diffusion, which allows a much faster spreading of a (bio)chemical state than pure diffusional processes. Mathematically they are described by reaction-diffusion (RD) equations [2]. In contrast to the standard diffusion equation, one-dimensional RD equations possess traveling solutions, which are states that travel with constant speed and constant shape. The simplest realization of these travelling waves is a chemical front, i.e., a wave that mediates transitions between two steady states. Fronts in reaction-diffusion systems have been thoroughly studied experimentally [3–6] and their properties agree well with analytical solutions and numerical simulations of RD systems [1,2,7].

In this paper we investigate fronts in an electrochemical system, i.e., a system in which the transport of chemical species can be due to both migration (motion of charged species due to an electric potential gradient) as well as diffusion (motion of species due to a concentration gradient). We will demonstrate that the movement of the fronts is due to electric potential gradients and that the global configuration of the electric potential leads to a global coupling that causes a nonconstant wave velocity.

The electrochemical reaction considered is the reduction of $S_2O_8^{2-}$ to SO_4^{2-} at a Ag electrode ($S_2O_8^{2-}+2e^-\rightarrow 2SO_4^{2-}$). This reaction consists only of basic electrochemical steps, i.e., the transport of the reactant ($S_2O_8^{2-}$) to the electrode and the exchange of electrons at the electrode (without chemical adsorption or any change of the electrode itself during the reaction, such as the formation of a passivating layer). Oscillations in this system have already been observed by Frumkin [8,9], who also proposed that the instability is a consequence of the recharging of the electrode: the driving force of reduction reactions usually *increases* with increasing negative overpotential (i.e., when a more negative potential is applied at the working electrode). However, if anions are reduced, as in our case, the electrostatic interaction between electrode and reactant can lead to a *decrease* in the reaction rate with increasing negative potential of the electrode close to the so-called point of zero charge, where the excess charge of the electrode changes from positive to negative. Such a negative differential resistance in the current-voltage characteristics is sufficient to give rise to oscillations or bistable behavior in some parameter interval in a system in which the voltage between the working and the reference electrode is held constant [10]. Wolf *et al.* [11] modeled the basic features of the experimentally observed current-potential characteristics qualitatively using a simple two variable model based on well-known electrochemical equations, taking into account the above mentioned additional electrostatic interaction. The aim of the present study is to investigate whether the instabilities of the global current densities are accompanied by spatial symmetry breaking.

EXPERIMENT

The experimental setup is shown in Fig. 1: Ag rings of different sizes embedded in a Teflon cylinder were used as working electrodes. They could be rotated at different speeds. The Ag rings had a width of 1 mm and a circumference of either 34.6 or 23.6 mm, so that the electrode may be viewed as "quasi-one-dimensional," the width being negligible compared to the circumference [Fig. 1(b)]. Before each experiment the Ag electrodes were pretreated using the same procedure as described in

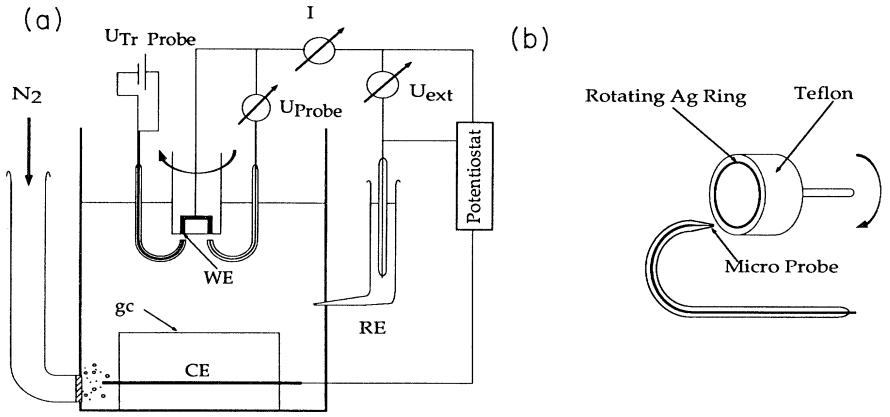

FIG. 1. (a) Scheme of the experimental setup; WE, working electrode; CE, counter electrode; RE, reference electrode (standard calomel electrode); gc, glass cylinder. Between WE and RE the voltage U_{ext} was held constant. The local potential in front of WE was measured by two micropotential probes. In some experiments one of them was exchanged by a trigger probe (see the text). (b) Enhanced sketch of working electrode and microprobes.

[11]. The electrochemical cell consisted of two compartments, the main compartment containing the working electrode and the Pt counter electrode (bent to a ring to ensure radial symmetry) remote from the working electrode [Fig. 1(a)]. The latter was shielded by a glass cylinder and N_2 was continuously bubbled through the cell through an inlet located near the counter electrode. A calomel reference electrode was placed in the second compartment, which was connected to the main compartment by a capillary. The voltage between the working electrode and the reference electrode was held constant during all experiments by means of a potentiostat. The base electrolyte was prepared with triply distilled water and consisted of $10^{-5}M$ H_2SO_4 [*pro analysi* (p.a.), Merck] with different amounts of Na_2SO_4 (p.a., Merck, 0.1–2 mM) and $Na_2S_2O_8$ (p.a., Merck, 0.1–5 mM).

The local potential in front of the electrode was recorded by two micropotential probes. The working electrode was rotated over the microprobes, thus allowing us to obtain a spatiotemporal picture of the potential distribution in front of the Ag ring. The local potential is a measure of the local current density, as a current through the electrolyte gives rise to an (Ohmic) potential drop. The micropotential probes consisted of Ag/AgCl microreference electrodes in glass tubes, which were pulled out to a capillary with an opening of approximately 200 μm in diameter. The end of the capillary was filled with NaCl-saturated agar-agar gel over which a saturated NaCl solution was placed in order to guarantee a fast response time. The end of the capillary was placed under the Ag ring, whereby the distance between the working electrode and the potential probe could be varied with a precision of 100 μm. Typical working distances were between 0.4 and 1 mm, well above the distance where either the transport of $S_2O_8^{2-}$ or the potential distribution would be disturbed through the probe. In order to study the response of the system to a local disturbance of the current (or potential) distributions, one of the potential probes was exchanged in some experiments with what we call a trigger probe, which is a glass tube into which two thin platinum wires are built. The end of the tube was again placed under the Ag ring in a distance of about 0.4–1 mm. Applying a short voltage pulse between the two wires leads to a brief disturbance of the local potential field.

RESULTS

Figure 2(a) displays the current-voltage characteristics of a 1 mM $S_2O_8^{2-}$ solution at different rotation rates of the electrode, i.e., different mass transfer rates. At low rotation rates the current exhibits oscillation in some in-

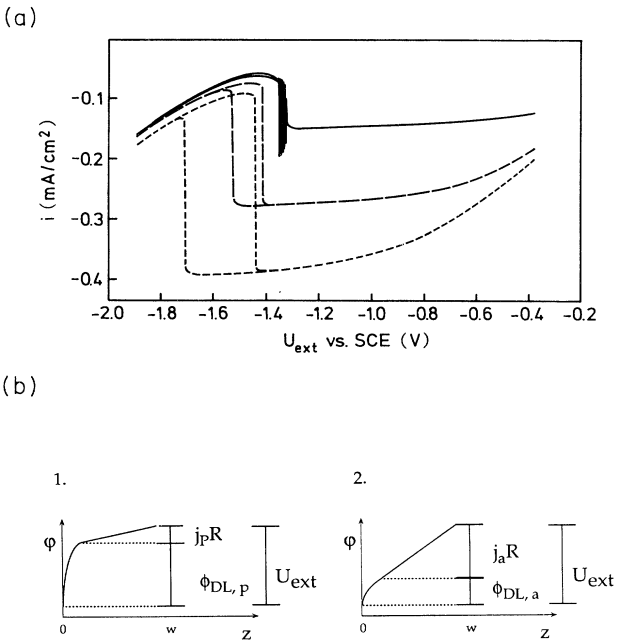

FIG. 2. (a) Current-voltage characteristics of a solution containing 1 mM $Na_2S_2O_8$ and 0.5 mM Na_2SO_4, with a pH of 5 at different rotation rates f of the electrode: solid curve, $f=5$ Hz, long-dashed curve, $f=20$ Hz; short-dashed curve, $f=40$ Hz. The current displays oscillations at low rotation rates and bistable behavior at higher rotation rates. (SCE denotes saturated calomel electrode.) (b) Schematics of the potential versus distance from the electrode for the two steady states in the bistable regime. w is the place of the reference electrode. The low current density (passive) state (1) is characterized by a large potential drop across the double layer ($\phi_{DL,p}$) and a small Ohmic potential drop. The high current density (active) state (2) is characterized by a small potential drop across the double layer ($\phi_{DL,a}$) and a large Ohmic potential drop.

terval of the externally applied voltage, whereas at high rotation rates bistable behavior is observed. The external voltage is composed of the potential drop across the double layer (ϕ_{DL}), which is a measure of the driving force of the reaction and the Ohmic potential drop in the electrolyte. Hence the different current densities of the two locally stable steady states in the bistable regime are connected with different potential drops across the double layer, as well as different concentrations of $S_2O_8^{2-}$ in front of the electrode [Fig. 2(b)]. In the following we call the state with the higher current density "active" and the one with the lower current density "passive" and we will concentrate on the spatiotemporal behavior of transitions from the passive to the active state.

The time trace of the current during a passive-active transition is shown in Fig. 3(a). Figure 3(b) displays the corresponding local potential as a function of space and time. (Due to surface inhomogeneities and imperfections in the ring width, there were small local potential inhomogeneities even in the spatially homogeneous steady states; hence the potential signal was determined relative to the steady state value and weighted by the global current.) At the beginning of the experiment the electrode was in a homogeneous state with low current density. Eventually, a fluctuation occurred that drove the system locally into the active state, forming a nucleation center [at the position π in Fig. 3(b)]. From this nucleus the active state expanded until the entire electrode acquired the high current density state. Obviously, the transition into the active state is connected with a spatial structure that is reminiscent of a traveling wave. While, however, in one-dimensional reaction-diffusion systems fronts travel with a constant speed, the velocity of the potential wave in Fig. 3(b) is not constant; rather it increases monotonically. The wave velocity at different times, as obtained from the potential probe readings, is shown as bars in Fig. 4. Once it is known that the transition is accompanied by fronts, their temporal evolution can also be obtained from the total current I: The differential change of the current I is given by

$$dI = j_a dA_a + j_p dA_p = j_a b(2v_F dt) + j_p b(-2v_F dt) ,$$

where j_a is the current density of the active state, j_p the current density of the passive state, A_a the area of the active state, and A_p the area of the passive state, respectively. v_F is the front velocity, b the width of the ring, and $(2v_F dt)$ the differential change of the distance covered since the nucleation of the front. Hence the front velocity at any time step can be obtained from the derivative of the global current. The dashed curve in Fig. 4 shows the velocity distribution of the data of Fig. 3(b) obtained from the total current [Fig. 3(a)]. This curve agrees reasonably well with the values obtained from the direct measurement (bars in Fig. 4).

The velocity distribution as well as the average velocity of the front was determined as a function of different parameters.

(a) The external voltage U_{ext}. Whereas the front shown in Fig. 3 was created through a fluctuation while sitting at a constant voltage, it was not practical to use this method when investigating the fronts as a function of U_{ext}, as the average time needed until a sufficiently large fluctuation spontaneously occurs becomes longer the further away the potential is from the saddle node bifurca-

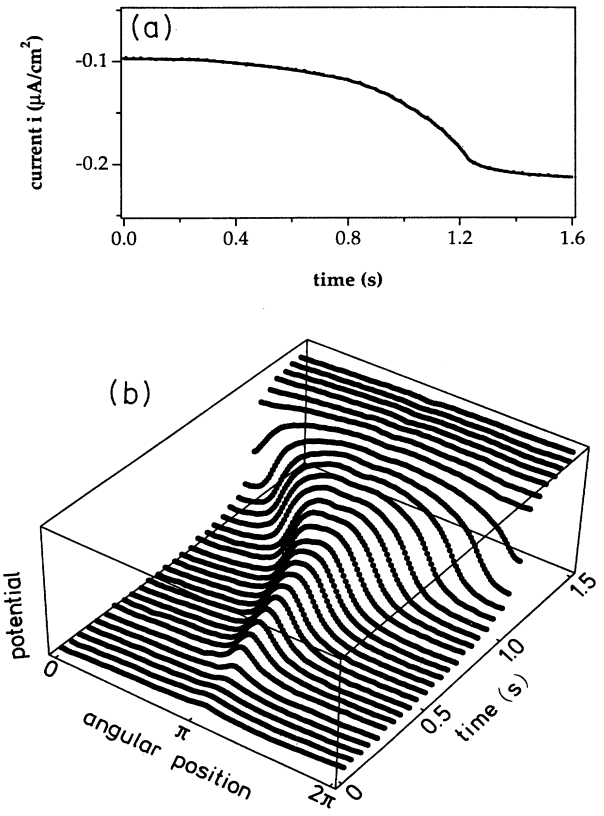

FIG. 3. (a) Time series of the total current i and (b) spatiotemporal plot of the local potential during a transition from the passive (low current density) to the active (high current density) state in the bistable regime at $U_{ext} = -1.36$ V, $f = 20$ Hz, $c_{Na_2S_2O_8} = 0.1$ mM, $c_{Na_2SO_4} = 0.1$ mM, and pH 5. The circumference of the electrode is equal to 3.46 cm.

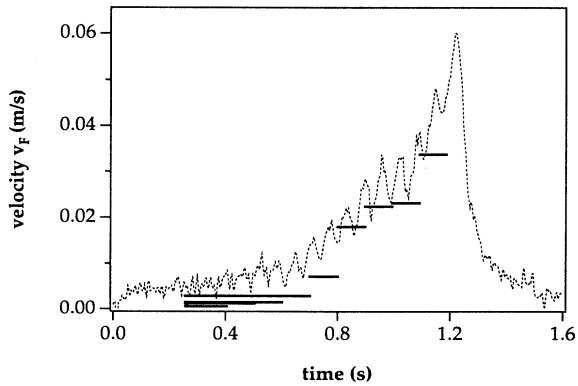

FIG. 4. Front velocity versus time for the transition displayed in Fig. 3. The bars show the mean velocity obtained from the micropotential probes. The dashed line displays the velocity obtained from the derivative of the current shown in Fig. 3(a).

tion, i.e., the border of the bistable regime (see, e.g., Fig. 2). Hence, for these measurements the transitions were triggered by imposing a short voltage pulse with the trigger probe. It was found that the amplitude of the pulse needed to induce a transition increased with increasing distance from the saddle node bifurcation until no transition at all could be induced. The average velocity increased in the same direction.

(b) The rotation frequency ω. Because the bistability is shifted with the rotation frequency (compare Fig. 2) towards different values of the applied voltage U_{ext} and the front velocity is a function of the voltage, or more importantly a function of the distance of the voltage from the saddle node bifurcation, U_{ext} was kept at equal distances from the saddle node bifurcation during these measurements. The average velocity of the front was only slightly affected by the rotation rate (at most 10%). This ensures that the wave is not affected by the forced convection of the electrolyte.

(c) The length of the ring. In order to corroborate that the acceleration of the front is not due to an initial effect stemming from a system size that is small compared to the characteristic pattern length, we used ring electrodes of two different diameters. Figure 5 displays a velocity distribution for the second electrode circumference that was used. Unquestionably, both velocity distributions (Figs. 4 and 5) are characterized by an increase of the front velocity with time during the whole transition, but obviously they have different functional dependences. Figure 5 shows an example of a front that is constantly accelerated for most of the time, whereas in Fig. 4 the increase of the velocity with time is larger than linear. These differences are not representative of the size of the ring. Rather they reflect different characteristics for different parameter values.

(d) The conductivity of the solutions (which is to a first approximation proportional to the ionic strength). A plot of the average velocity of the fronts versus the conductivity of the solution is shown in Fig. 6. It can be seen that the velocity increases strongly with increasing conductivity. At constant conductivity, different ratios of Na_2SO_4 and $Na_2S_2O_8$ concentrations were used in order

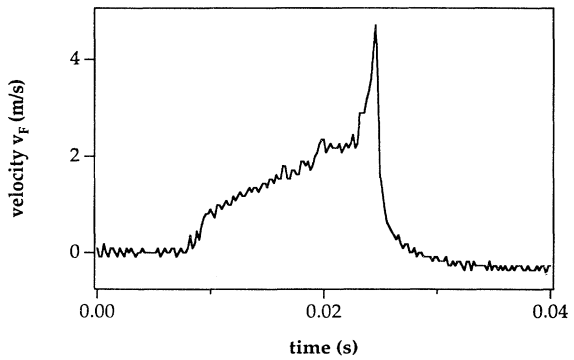

FIG. 5. Front velocity versus time of a passive-active transition at $U_{ext}=-1.27$, $f=30$ Hz, $c_{Na_2SO_4}=2$ mM, $c_{Na_2SO_4}=1$ mM, and pH 5. The circumference of the electrode is equal to 2.36 cm.

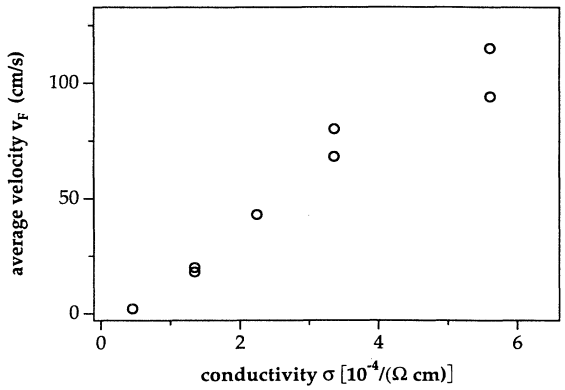

FIG. 6. Average front velocity as a function of the electrolyte conductivity σ. The conductivity was obtained using the following dependency: $\sigma=(F^2D/RT)\sum_i z_i^2 c_i$. F, Faraday constant; D, diffusion coefficient (10^{-5} cm^2/s); R, universal gas constant; T, absolute temperature; z_i, charge numbers; c_i, concentrations.

to estimate the effect of the $S_2O_8^{2-}$ concentration in the electrolyte. For example, the two points shown at $\sigma=5.6\times10^{-4}$ $(\Omega\,\mathrm{cm})^{-1}$ were obtained using 0.5 mM $Na_2S_2O_8$, and 2 mM Na_2SO_4 and 2.0 mM $Na_2S_2O_8$, 0.5 mM Na_2SO_4, respectively. The velocities differ only slightly, whereas at the lower conductivity $\sigma=1.3\times10^{-4}$ $(\Omega\,\mathrm{cm})^{-1}$, where the concentration of the reactant $S_2O_8^{2-}$ was again 0.5 mM, but the concentration of Na_2SO_4 only 0.1 mM, the front velocity fell to one-fifth of its value at $\sigma=5.6\times10^{-4}$ $(\Omega\,\mathrm{cm})^{-1}$.

DISCUSSION

The experiments show that the transitions in the bistable regime are mediated by fronts, i.e., they occur spatially nonhomogeneously. The velocity of the fronts increases with time, i.e., the fronts are accelerated. The acceleration does not depend on the length (circumference) of the electrode and should therefore be an intrinsic property of the system rather than an initial effect. The average velocity is not affected appreciably either by the concentration of the reactive species (at constant conductivity) or by the rotation rate of the electrode, but depends strongly on the conductivity of the electrolyte.

These results point out two differences of this system and, as we will discuss below, of electrochemical systems in general, from "usual" reaction-diffusion systems. The first difference is the mechanism by which information is spatially transmitted. The only parameter that drastically effects the velocity of the front is the conductivity of the electrolyte and the only process that is affected by the conductivity is migration. As is shown in Fig. 2(b), the two stable states are characterized by different potential drops across the electrode-electrolyte interface, which are connected with the different current densities of these states and different concentrations of the reactive species. The potential drop between the two states (across the interface) leads to migration currents, whereas the concentration gradient leads to diffusion currents. The experi-

ments suggest that the movement of the front is induced by local migration currents across the interface rather than by diffusion currents. Let us consider the relations at the interface more closely. Figure 7 shows a sketch of the front. As a high current density corresponds to a low $S_2O_8^{2-}$ concentration in front of the electrode and a low current density, conversely, to a high concentration, $S_2O_8^{2-}$ diffuses from the passive to the active state. This leads to a higher concentration ahead of the active part of the front (dotted line in Fig. 7), which in turn increases the reaction rate and thus leads to an even higher current density in the active state and hence to a lower potential drop. Consequently, diffusion causes a stabilization of the front rather than its motion (dashed line). The electric field across the interface, on the other hand, has the opposite effect: Anions migrate from the active to the passive state and cations in the reverse direction. This increases the potential in front of the active state and lowers it in front of the passive state (dotted line in Fig. 7; see also below). These changes in the local potential lead to higher reaction rates in front of the passive state and to lower reaction rates in front of the active state and thus drive the expansion of the more stable of the two states (dashed line).

The second difference is the observation of an acceleration during the transition between the passive and the active state, which is not expected in bistable reaction diffusion systems. So far, we have seen that the movement of the front is caused by migration currents parallel to the electrode, which lead to a lowering of the potential in front of the passive state and a higher potential in front of the active state. These migration currents are, however, not the only mechanism that leads to a change of the potential in front of the electrode. During the transition, more and more of the area of the ring is covered by the active state and therefore the total current increases. The currents in the electrolyte are determined by the gradient of the electric potential. The potential at every point in the electrolyte, and thus also in front of the interface, depends on the potential distribution of the *whole* electrode area. This means that all parts of the electrode are globally coupled.

Consideration of potential and current distributions in the electrolyte in more detail yields a more precise picture of the origin of this coupling. Let us assume that during the transition there is one part of the electrode in the active state, the other part in the passive state, and that the two states are connected via an interface. At some remote distance from the electrode all potential inhomogeneities will be smoothed out and the potential distribution is homogeneous. The value of the potential in the electrolyte is given at the place of the reference electrode $z=w$ (which has to be at a distance from the reference electrode at which the potential is homogeneous). Since outside the electrochemical double layer the solution is (in a good approximation) electroneutral, the potential distribution is governed by the Laplace equation. Hence, for a given potential difference between the working and the reference electrode and a potential distribution at the working electrode, we can calculate the potential distributions and all migration currents inside the bulk electrolyte (outside the electrochemical double layer). In Fig. 8 the calculated potential distribution in the electrolyte at a constant distance from the electrode z_1 is shown for different ratios of active and passive area of the electrode and realistic values of the potential at the electrode and at $z=w$. The easiest assumption is that different ratios of the two states are traveled through with progressive time in the experiment and thus Fig. 8 can be compared to Fig. 3(b). Both plots exhibit striking similarities, e.g., in both plots the height of the potential at x values at which the electrode is in its active state increases with increasing total active area until approximately half of the electrode is in the active state. A simi-

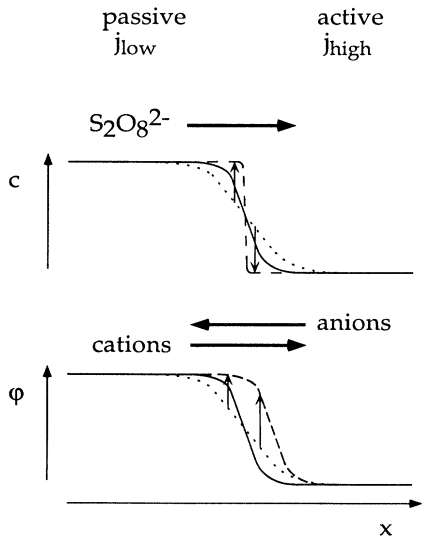

FIG. 7. Schematic drawing of concentration and potential profile of a front. The passive (active) state is characterized by a high (low) $S_2O_8^{2-}$ concentration and a high (low) potential. The concentration gradient leads to a steepening of the front, whereas the electric field induces its motion (see the text).

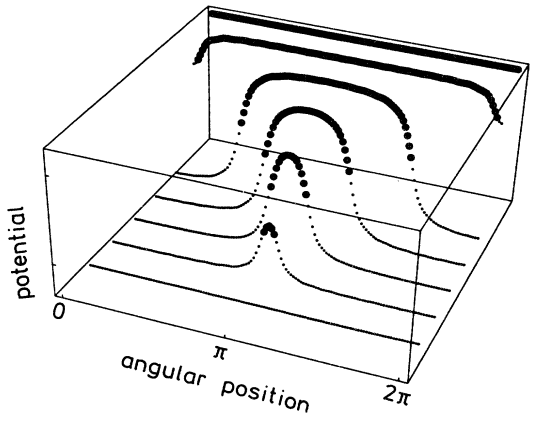

FIG. 8. Calculated potential distribution in the electrolyte at a constant distance $z_1=1$ mm from the electrode for different portions of the active and the passive state at the boundary (electrode). The thick dots mark the position that was set in the passive state at the electrode. Note the similarity to Fig. 3.

lar picture is obtained if for one length ratio of the active and the passive state at the electrode the calculated electrolyte potential is plotted as a function of the distance from the electrode as shown in Fig. 9. With the help of this figure it is easy to put the global coupling in a quantitative context. Consider the migration currents between the working and the reference electrode within a small interval Δx as indicated in Fig. 9. The electrode can be thought of as a capacitance connected in parallel to a resistance. Hence the current through the interface at $z=0$ is composed of a Faradaic contribution j_F due to the reaction and a capacitive contribution j_C, which leads to the charging of the electrode. At $z=w$, the homogeneous potential distribution leads to a leveling of the current distribution and we can approximate the current density in our slice Δx at $z=w$ by the average current density

$$(\Delta x)j(x)|_{z=w} \approx \frac{\Delta x}{2\pi}\int j(x)|_{z=w}dx=(\Delta x)\bar{j} \ .$$

As in the slice Δx the currents through the line elements at the working and the reference electrode differ by the nonhomogeneous cross currents in x direction j_x, the potential change of the portion Δx of the electrode is given by (see also [12])

$$\begin{aligned} j_C &= C\frac{\partial\phi(x)}{\partial t} \\ &= \bar{j}-j_R \\ &\quad + \frac{1}{\Delta x}\int \left[j_{\mathrm{mig}}(z)\Big|_{x+\Delta x/2} - j_{\mathrm{mig}}(x)\Big|_{x-\Delta x/2} \right] dz \ . \end{aligned} \tag{1}$$

Equation (1) contains two terms that possess global character: $\bar{j}$ and the integral over the difference of the migration currents. The average current density $\bar{j}$ has the same effect on the dynamics of all parts of the electrode, no matter how far apart they are from the front, and is thus completely global in nature. In order to understand the effect of this term on the dynamics better, let us do a gedanken experiment. Suppose we know the potential values and the current densities of the two steady states in the bistable regime. Now we construct an initial condition such that one part of the electrode is in one of the steady states and the other part in the other one and neglect for a moment the migration currents parallel to the electrode. Obviously, the average current density of the system is different from either current density of the steady states and hence our initial condition will develop with time either into one of the homogeneous steady states or into some other spatially structured attractor that may exist. As there is no local exchange of information across the interface, all parts of the electrode that are in the same state will show the same temporal dynamics and hence the transition will appear homogeneous. The integral term over the migration currents in x direction, on the other hand, obviously contains local transmission of information parallel to the electrode. It possesses, however, also global information. The potential at every point in the electrolyte is given by the Laplace equation and is thus influenced by the potential distribution of the *whole* electrode. In contrast to the average current density, the contribution of this term to different parts of the electrode is, however, different. Therefore, this type of global coupling is more precisely described as *nonlocal*. Calculations of the integral for different ratios of the electrode in the two states showed

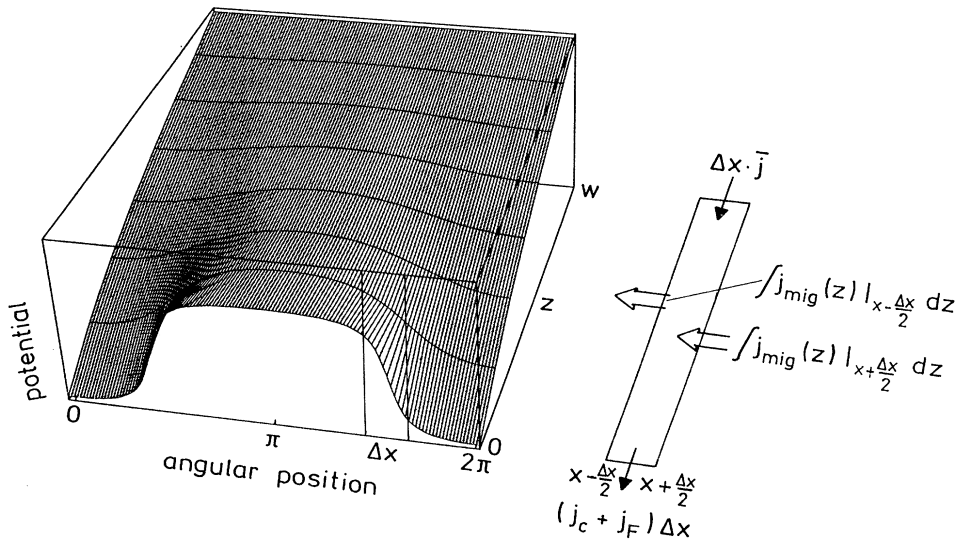

FIG. 9. Calculated potential distribution in the electrolyte as a function of the distance from the electrode z for a homogeneous potential at $z=w$ and adjacent passive or active regions at the electrode ($z=0$). Consider a line segment Δx between the working and the reference electrode ($z=w$). The potential distribution implies migration currents in the x and the z direction. The sum over these currents is equal to the currents through the working electrode, which are composed of a capacitive j_C and a reaction current j_F. Therefore the charging of the electrode can be calculated from such a potential distribution and explains the origin of the acceleration of the fronts (see the text).

that (a) the contribution of this term is much larger in the interface region than outside the interface and considerably larger than the one of the average current density $\bar{j}$ and (b) the temporal change of the potential in the interface becomes faster during the transition [13]. The first point ensures that fronts exist at all and the second one leads to an accelerated motion whose origin lies in the nonlocal character of this term.

During the transition the current density increases and, as an increasing total current leads to a faster spread of the active state, and hence to its own "production," we call the nonlocal coupling "positive." Another example of accelerated wave phenomena in an electrochemical system has been reported by Otterstedt, Jaeger, and Plath [14], who studied spatiotemporal patterns during the electrodissolution of cobalt. The authors discuss several possible origins of these accelerated waves; future experiments will show whether they can also be explained by such a nonlocal coupling [15].

So far we have argued that the important transport mechanism that leads to the movement of the fronts is migration and that there exists a nonlocal coupling that constitutes a positive feedback. Any spatial inhomogeneities in an electrochemical system lead to an inhomogeneous potential distribution and hence to migration currents parallel to the electrode. Consequently, the governing equations that describe pattern formation in all electrochemical systems are reaction-*migration*-diffusion systems. This additional transport mechanism adds new aspects to pattern formation in chemical systems.

Recently the influence of an electric field on patterns in homogeneously catalyzed chemical systems, such as, for example, the Belousov-Zhabotinsky reaction, was studied [16–21]. It could, e.g., be shown that the front velocity can be tuned by the strength of an electric field [18] or that the electric field might give rise to Turing patterns under conditions under which they are not expected at zero field strength [21]. Münster *et al.* [20] demonstrated that the electric field can induce transitions between stationary and oscillatory states as well as between striped and hexagonal patterns. To what extent the patterns of these systems, in which the electric field is a parameter, can also be found in electrochemical systems, in which the electric potential is a variable, is an interesting, though still open, question.

The considerations of how the current density gives rise to a positive global coupling were completely general. This means that such a *global* coupling exists in any electrochemical system in which the external voltage is held constant. Recently, more and more attention has been paid to the influence of a global interaction between spatially averaged quantities and the reaction dynamics in reaction-diffusion systems [22–28]. Zhukov and Barelko [22] introduced a heating constraint on the average temperature in a nonisothermal heterogeneously catalyzed system and observed standing fronts in the bistable regime of the reaction. Such stationary fronts were also realized in a chain of 128 coupled oscillators [29]. In both experiments there was a constraint that gives rise to a negative feedback of the coupling parameter and the observations are just the counterpart of the accelerated fronts that we observed for a positive global feedback. In electrochemical systems a negative global feedback can be realized under galvanostatic conditions, under which Lev *et al.* [30] found antiphase oscillations on a Ni wire, which are similar to the ones Middya and Luss [26] found in calculations of nonisothermal reactions held at a constant (average) temperature.

In conclusion we have shown that the fronts observed during the reduction of peroxodisulfate in the bistable regime are caused by migration, i.e., movement of ions in an electric field, and their acceleration is due to a positive nonlocal coupling through the electric field. Our considerations show that migration and global coupling are the important features that govern patterns in most electrochemical systems. The studies of the interaction of migration and reaction as well as the role of global coupling terms are certainly still in the initial stages and it can be assumed that they will reveal a rich variety of chemical wave phenomena.

ACKNOWLEDGMENTS

The steady interest and support by G. Ertl was particularly helpful during this work. We are very grateful to K. Doblhofer for many fruitful discussions and thank A. Zhabotisnky for his stimulating remarks during his visit in Berlin. We also thank K. Grabitz and S. Plass for their technical assistance. The financial support from the Deutsche Forschungsgemeinschaft is acknowledged.

[1] J. D. Murray, *Mathematical Biology* (Springer, Berlin, 1990).
[2] A. S. Mikhailov, *Foundations of Synergetics I* (Springer, Berlin, 1990).
[3] R. H. Harding and J. Ross, J. Chem. Phys. **92**, 1936 (1990).
[4] A. Saul and K. Showalter, in *Oscillations and Traveling Waves in Chemical Systems,* edited by R. J. Field and M. Burger (Wiley, New York, 1985).
[5] J. Harrison and K. Showalter, J. Phys. Chem. **90**, 225 (1986).
[6] V. v. Barelko, I. I. Kurochka, A. G. Merzhanov, and K. G. Shkadinskii, Chem. Eng. Sci. **33**, 805 (1978).
[7] F. Schlögl, Z. Phys. B **253**, 147 (1972).
[8] A. Frumkin, O. A. Pettrii, and N. V. Nikolaeva-Fedorovich, Dokl. Akad. Nauk. SSSR **136**, 1158 (1961) [Proc. Acad. Sci. USSR Phys. Chem. Sec. **136**, 183 (1961)].
[9] A. Frumkin, Z. Elektrochem. **59**, 807 (1955).
[10] M. T. M. Koper, Electrochim. Acta **37**, 1771 (1992).
[11] W. Wolf, J. Ye, M. Purgand, M. Eiswirth, and K. Doblhofer, Ber. Bunsenges. Phys. Chem. **96**, 1797 (1992).
[12] M. T. M. Koper and J. H. Sluyters, Electrochim. Acta **38**, 1535 (1993).
[13] G. Flätgen and K. Krischer (unpublished).
[14] R. D. Otterstedt, N. I. Jaeger, and P. J. Plath, Int. J. Bifurcation Chaos **4**, 1265 (1994).

[15] Another example of accelerating chemical waves was observed by Mikii *et al.* in the Belousov-Zabotinsky reaction. In parallel with the chemical wave, hydrodynamic motion was observed, and in this case the acceleration is most likely due to a coupling of hydrodynamics with the reaction-diffusion system: H. Mikii, H. Yamamoto, S. Kai, and S. C. Müller, Phys. Rev. E **48**, R1627 (1993).
[16] R. Sultan and P. J. Ortoleva, J. Chem. Phys. **92**, 1062 (1990).
[17] P. Ortoleva, Physica D **26**, 67 (1986).
[18] H. Sevcikova and M. Marek, Physica D **9**, 140 (1983).
[19] H. Sevcikova, M. Marek, and S. C. Müller, Science **257**, 951 (1992).
[20] A. F. Münster, P. Hasal, D. Snita, and M. Marek, Phys. Rev. E **50**, 546 (1994).
[21] H. Malchow, Z. Phys. Chem. **271**, 751 (1990).
[22] S. A. Zhukov and V. V. Barelko, Sov. J. Chem. Phys. **4**, 883 (1982).
[23] Y. Volodin, V. N. Zvyagin, A. N. Ivanova, and V. V. Barelko, Adv. Chem. Phys. **77**, 551 (1990).
[24] L. Schimansky-Geier, Ch. Zülicke, and E. Schöll, Physica A **188**, 436 (1992).
[25] F. Mertens, R. Imbihl, and A. Mikhailov, J. Chem. Phys. **99**, 8668 (1993); **101**, 9903 (1994).
[26] U. Middya and D. Luss, J. Chem. Phys. **100**, 3568 (1994).
[27] U. Middya and D. Luss, J. Chem. Phys. **100**, 6386 (1994).
[28] M. Falcke and H. Engel, Phys. Rev. E **50**, 1353 (1994).
[29] M. Bode, A. Reuter, R. Schmeling, and H.-G. Purwins, Phys. Lett. A **185**, 70 (1994).
[30] O. Lev, M. Sheintuch, L. M. Pismen, and Ch. Yarnitzky, Nature **336**, 488 (1988).